# Reaction enhancement of isolated scalars by vortex stirring

John P. Crimaldi,[1,a)] Jillian R. Cadwell,[1] and Jeffrey B. Weiss[2]
[1]*Department of Civil and Environmental Engineering, University of Colorado, Boulder, Colorado 80309-0428, USA*
[2]*Department of Atmospheric and Oceanic Sciences, University of Colorado, Boulder, Colorado 80309-0311, USA*

(Received 24 April 2008; accepted 26 June 2008; published online 31 July 2008)

The effect of vortex stirring on reaction rate enhancement is investigated for two reactive scalars initially separated by a third nonreactive scalar. The presence of the intervening scalar precludes reactions at early times. Vortex stirring accelerates the coalescence of the reactive scalars relative to pure diffusion and enhances the resulting reaction rates. Analytical and numerical results for reactive stirring by a single point vortex are shown for a range of Péclet (Pe) and Damköhler (Da) numbers. At low Da and high Pe, nondimensional reaction rates grow as $\mathrm{Pe}^{1/3}$, and peak reaction times decrease as $\mathrm{Pe}^{-2/3}$. Reaction rates scale linearly with Da for slow reactions, but this scaling breaks down for fast reactions due to reactant depletion. The stirring-induced reaction rate enhancement is shown to be relatively insensitive to initial placement of scalars within the point vortex. The study provides mechanistic insights into more general mixing and reaction problems involving initially isolated scalars. © *2008 American Institute of Physics*. [DOI: 10.1063/1.2963139]

## I. INTRODUCTION

An understanding of the mechanisms by which vortices stir and mix scalars is fundamental to the prediction of reaction rates in reactive fluid flows. From simple laminar flows to chaotic or turbulent processes, vortices are associated with rapid mixing. Vortical structures enhance scalar dissipation and mixedness through a coupling between kinematic straining and molecular diffusion. When reactive scalars are present within the structures, local reaction rates are also enhanced.

It is common to investigate the mechanistic features of complex vortex-driven mixing processes with simple planar models involving an isolated vortex or several interacting vortices.[1–9] While scaling relationships from these simple models often do not extrapolate well to three-dimensional, chaotic, or turbulent flows, the simple models elucidate instantaneous processes seen locally in more complex flows. Frequently, simple models exhibit complex behaviors that are interesting in their own right.

Reactive mixing problems can be classified based on the initial topology of their scalar fields. One class, which encompasses most studies in the current literature,[10–21] involves two reactive scalars that together fill the entire domain and are initially in contact with one another along a material interface (see examples in Fig. 1). The scalars react immediately due to molecular diffusion at the shared interface. In the presence of vortex stirring, interfacial stretching increases scalar mixedness,[1,2,8] accelerates scalar dissipation,[4] and enhances reaction rates.[9] It is useful to note that in nonreactive mixing scenarios, problems in this first topological class are indistinguishable from single-scalar mixing problems. Nondimensionalizing the two scalar concentrations $C_A$ and $C_B$ as mass fractions gives $C_A+C_B=1$ everywhere. Writing $C=C_A$ with $1-C=C_B$ permits the problem to be formulated in terms of a single species equation.[1]

A second class of reactive mixing problems, which has received scant attention in literature, involves two reactive scalars that do not initially share a material interface due to the intervening presence of a third nonreactive fluid (see examples in Fig. 2). Reaction rates in this case are initially zero, but are nonzero at intermediate time scales in the presence of molecular diffusion. The effect of stirring on reactions rates for this class of problems is less clear. In fact, it is possible to envision stirring scenarios that *reduce* reaction rates (again, relative to the purely diffusive case). The effect of vortex stirring on reaction rates for this second class of problems is the central question for the present paper. In particular, we are interested in predicting reaction rates inclusive of instantaneous structured stirring relative to rates predicted using an effective eddy diffusivity as a surrogate for the stirring field. Following the lead of previous mixing studies, we limit our investigation to the simplest possible case of stirring by a single two-dimensional vortex. The goal is to establish a foundation for understanding this second class of problems by elucidating the mechanistic mixing and reaction processes at the scale of the vortex.

Straining mechanisms associated with the momentum field are clearly independent of the topological class of the initial scalar field. Kinematic straining determines the growth rate of material lines, which, in turn, governs the rate at which scalar fluctuations are dissipated. For a two-dimensional incompressible flow such as a point vortex, material lines grow linearly as $\gamma t$, where $\gamma$ is the local strain rate. A scalar patch [as in Fig. 1(b) or 2(b)] near an isolated point vortex forms a spiral scalar structure that dissipates with a mixing time that scales as $\gamma^{-1}\,\mathrm{Pe}^{1/3}$, where Pe is a vortex Péclet number.[4,5,7,22] The present study demonstrates

a)Author to whom correspondence should be addressed. Electronic mail: crimaldi@colorado.edu.

 

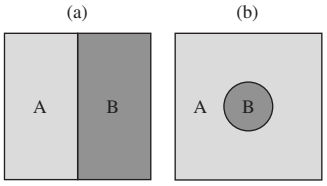


FIG. 1. Examples of initial scalar topologies in a square domain corresponding to the first class of problems discussed in the text. Two scalars denoted $A$ and $B$ fill the entire domain and share a material interface.

that this $\mathrm{Pe}^{1/3}$ dissipation scaling extends to the scaling of reaction rates even for problems in the second topological class.

We were initially motivated to study reactions in the second topological class by an interesting biological process. Many marine invertebrates (e.g., corals, urchins, and anenomes) reproduce sexually via a process called broadcast spawning.[23] Males and females synchronously release sperm and egg, respectively, from separate locations on the sea bed. The process subsequently relies on structured stirring from turbulence and vortex-dominated bedform wakes to bring gametes into close proximity such that fertilization might occur. Topologically, the sperm and egg are the two reactive scalars, initially separated by inert gamete-free water. Models of this process based on effective eddy diffusivities vastly underpredict observed fertilization rates.[24] We hypothesized that details of the instantaneous scalar fields (absent in the eddy diffusion models) were critical to the prediction of fertilization rates.[25] In an earlier study,[26] we calculated reaction rates in the low-Damköhler limit for two initially distinct scalars in a point vortex flow. Peak reaction rates for this problem in the second topological class scaled as $\mathrm{Pe}^{1/3}$, with the peak reaction time scaling as $\mathrm{Pe}^{-2/3}$. In the present paper, we expand that study to include the effect of reaction kinetics at finite Damköhler numbers.

## II. PROBLEM DESCRIPTION

Geometric details of the problem are shown in Fig. 3. A single two-dimensional vortex $u_\phi(r)$ stirs two reactive point-source scalars $A$ and $B$ placed within an inert background fluid. The scalars are initially located at radii $R_A$ and $R_B$ from the vortex center, separated by angle $\phi$ and distance $L$. Both scalars have molecular diffusivity $D$ and initial mass $M$. Deviations from axial symmetry are described by two nondimensional eccentricities. The angular eccentricity is simply

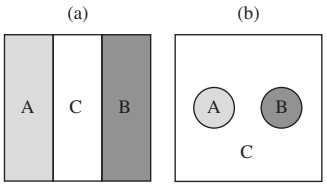


FIG. 2. Examples of initial scalar topologies corresponding to the second class of problems. Two reactive scalars $A$ and $B$ are initially separated by a nonreactive fluid, denoted as $C$.

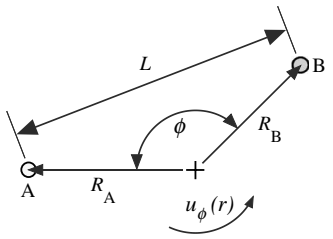


FIG. 3. Geometric definitions for the initial scalar condition. Point masses of reactive scalars $A$ and $B$ (shown here for clarity as finite-size blobs) are placed within an inert background fluid and stirred by a vortex centered on the + symbol.

$\phi$, where $0 \leq \phi \leq \pi$, with $\phi = \pi$ corresponding to the symmetric case with scalars in diametric opposition. The radial eccentricity is defined as

$$E = \frac{|R_A - R_B|}{R_A + R_B}, \tag{1}$$

where $0 \leq E \leq 1$, $E=0$ is the symmetric case $R_A = R_B$, and $E=1$ corresponds to the limit where either $R_A/R_B$ or $R_B/R_A \to 0$. Pictorial interpretations of intermediate and limiting $E$ values are shown in Fig. 4.

Analytical and numerical techniques are used to calculate the reaction rate between scalars $A$ and $B$ for a range of eccentricities, Péclet, and Damköhler numbers. Except where noted, the flowfield is a point vortex with circulation $\Gamma$,

$$u_\phi(r) = \frac{\Gamma}{2\pi r}. \tag{2}$$

A synthesis reaction $A + B \to AB$ is used with second-order reaction rate kinetics.

## III. GOVERNING EQUATIONS

Each of the two scalars $A$ and $B$ is governed by a dimensional reactive advection-diffusion equation of the form

$$\frac{\partial \tilde{C}}{\partial \tilde{t}} = -\tilde{\mathbf{u}} \cdot \nabla \tilde{C} + D\nabla^2 \tilde{C} - \tilde{\theta}, \tag{3}$$

where the three terms on the right-hand side express Eulerian concentration changes due to advection, molecular diffusion, and reaction. The two scalar concentrations are coupled by a second-order dimensional reaction term

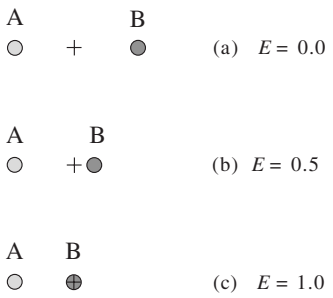


FIG. 4. Interpretation of the radial scalar eccentricity $E$ for $R_A \geq R_B$ and $\phi = \pi$, showing (a) the limiting symmetric case $E=0$, (b) an intermediate case $E=0.5$, and (c) the limiting asymmetric case $E=1$.

$$\tilde{\theta} = k\tilde{C}_A\tilde{C}_B, \tag{4}$$

where $k$ is a reaction constant. Concentrations are then nondimensionalized by $M/L^2$, lengths by $L$, and velocities by $U=u_\phi(R)$, where $R=(R_A+R_B)/2$. Time is nondimensionalized as

$$t = \frac{\tilde{t}}{t_d}, \tag{5}$$

where $t_d=L^2/8D$ is a diffusive time scale that corresponds to the peak reaction time for the purely diffusive case (Pe=0) in the slow reaction limit (Da$\ll$1). Finally, advective and reactive time scales are defined as $t_a=R/U$ and $t_r=L^2/kM$. The governing equations for the coupled scalar dynamics can then be expressed nondimensionally as

$$\begin{aligned}\frac{\partial C_A}{\partial t} &= -\frac{\alpha}{2}\mathrm{Pe}\,\mathbf{u}\cdot\nabla C_A + \frac{1}{8}\nabla^2 C_A - \theta,\\ \frac{\partial C_B}{\partial t} &= -\frac{\alpha}{2}\mathrm{Pe}\,\mathbf{u}\cdot\nabla C_B + \frac{1}{8}\nabla^2 C_B - \theta,\end{aligned} \tag{6}$$

where $\theta$ is the nondimensional reaction rate;

$$\theta = \mathrm{Da}\, C_A C_B, \tag{7}$$

the Damköhler number is

$$\mathrm{Da} = \frac{t_d}{t_r} = \frac{kM}{8D}, \tag{8}$$

and the Péclet number is

$$\mathrm{Pe} = \frac{t_d}{t_a} = \frac{L^2U}{8DR}. \tag{9}$$

For a point vortex, Eqs. (2), (10), and (9) combine to give $\mathrm{Pe}=\Gamma/(4\pi\alpha^2 D)$. The geometric parameter $\alpha$ in Eq. (6) is simply

$$\alpha = 2R/L. \tag{10}$$

Note that $\alpha$ is of the order of unity except when $\phi\to 0$.

The total dimensional reaction rate integrated over the entire domain $\tilde{A}$ is

$$\tilde{\Theta} = \int\int \tilde{\theta}\, d\tilde{A}, \tag{11}$$

which, for convenience, is nondimensionalized as

$$\Theta = \pi e \int\int \theta\, dA = \frac{\pi e}{8}\frac{L^2}{MD}\tilde{\Theta}. \tag{12}$$

Analytical and numerical solutions for the nondimensional integrated reaction rate $\Theta$ are given in Secs. IV and V, respectively.

## IV. ANALYTICAL SOLUTIONS FOR SLOW REACTION LIMIT (Da$\ll$1)

Analytical expressions for $\Theta$ are given for the limiting cases Pe=0 and Pe$\gg$1, both in the case of the slow reaction limit (Da$\ll$1). The slow reaction limit simplifies analytical solutions by decoupling the system of scalar equations in Eq. (6). The analytical solutions provide insights into relevant scaling relationships and serve to validate numerical simulations in Sec. V.

### A. Purely diffusive (Pe=0)

For the case of a purely diffusive system (Pe=0) in the slow reaction limit (Da$\ll$1), Eq. (6) reduces to a pair of uncoupled diffusion equations with simple analytical solutions. This permits an analytical solution to the nondimensional integrated reaction rate [Eq. (12)], given by

$$\Theta(t) = \mathrm{Da}\frac{e}{t}\exp\left(-\frac{1}{t}\right). \tag{13}$$

The solution has a maximum $\Theta_{\mathrm{peak}}=\mathrm{Da}$ occurring at $t=1$, as shown in Fig. 6(a). This diffusive reaction rate solution serves as a baseline for the effect of vortex stirring in subsequent solutions and simulations.

### B. Strongly advective (Pe$\gg$1)

For the limiting case of a strongly advective system (Pe$\gg$1), again in the slow reaction limit, an analytical solution for $\Theta$ can be determined by posing the problem in terms of stochastic differential equations. For simplicity, only the symmetric initial condition ($E=0$, $\phi=\pi$) is considered. Working in local Cartesian coordinates $\mathbf{x}=(x_1,x_2)=(r\phi, r-R)$, $\mathbf{u}=(u_1,0)$, the concentration of a collection of scalar particles initially lumped at $\mathbf{x}=(0,0)$ is a bivariate Gaussian distribution written as[27]

$$C(\mathbf{x},t) = \frac{M}{2\pi}\sqrt{\det\mathbf{A}}\,\exp\left(-\frac{1}{2}\mathbf{x}\cdot\mathbf{A}\cdot\mathbf{x}\right), \tag{14}$$

where $\mathbf{A}$ is a tensor whose inverse is the covariance tensor of the scalar particle distributions $\mathbf{X}$,

$$A_{ij}^{-1} = \langle (X_i - \langle X_i\rangle)(X_j - \langle X_j\rangle)\rangle. \tag{15}$$

The high-Pe limit restricts diffusive scalar excursions in $x_2$ to be small over advective time scales, allowing the shearing velocity profile to be linearized about $x_2=0$ to $u_1=U+2\sigma x_2$, with constant shear $\sigma=\Gamma/\pi R^2=8\,\mathrm{Pe}\,D/L^2$. The 2 in front of the shear is a geometrical factor resulting from the transformation from polar to local Cartesian coordinates. Particle velocities can thus be written as

$$\begin{aligned}\dot{X}_1 &= U - 2\sigma X_2(t) + \xi_1(t),\\ \dot{X}_2 &= \xi_2(t),\end{aligned} \tag{16}$$

where diffusion is modeled via a random Gaussian process $\boldsymbol{\xi}=(\xi_1,\xi_2)$ with ensemble mean $\langle\xi_i(t)\rangle=0$ and variance $\langle\xi_i(t)\xi_j(t)\rangle=2D\delta_{ij}\delta(t)$. The velocity equations can be integrated to give the moments of the particle locations, yielding

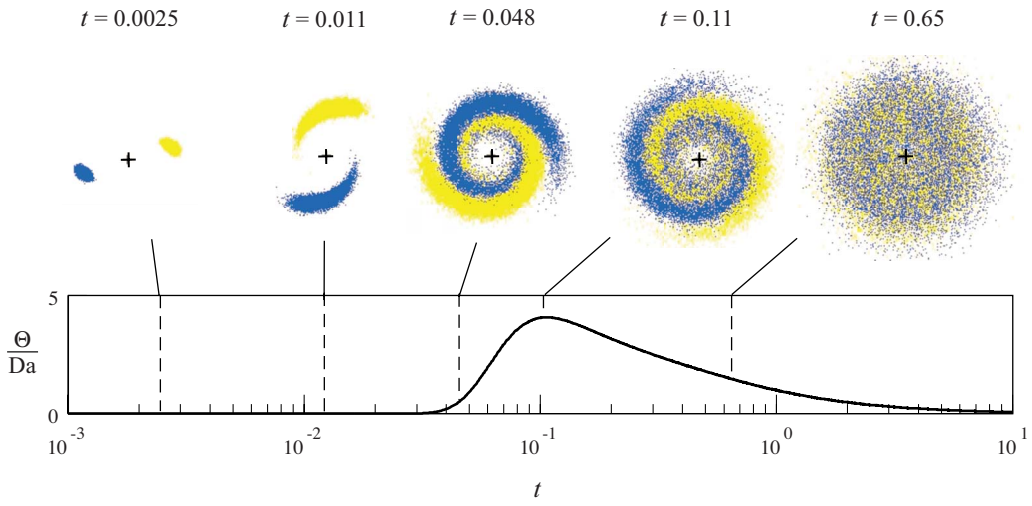


FIG. 5. (Color online) Particle locations at five simulation times for scalars $A$ [light gray (yellow online)] and $B$ [dark gray (blue online)] for the case Pe $=100$, Da$=1$, with symmetric initial condition $E=0$ and $\phi=\pi$. Also shown is the associated $\Theta$ vs $t$ simulation result for a continuous range of times with the corresponding snapshot times indicated as dashed lines.

$$\mathbf{A}^{-1} = 2Dt\begin{bmatrix} \frac{1}{3}\sigma^2 t^2 & -\frac{\sigma}{2}t \\ -\frac{\sigma}{2}t & 1 \end{bmatrix}. \tag{17}$$

The $A_{11}^{-1}$ term displays the well-known $t^3$ shear dispersion; this term also has a linear diffusion term that is negligible at high Pe for the times of interest and is dropped.

The transformation to Cartesian space requires the use of periodic image sources in the $x_1$ direction. Thus, the two scalar sources at $(r,\phi)=(R,0)$ and $(R,\pi)$ are represented in Cartesian space by sources at $\mathbf{x}=(n2\pi R,0)$ and $(\pi R+n2\pi R,0)$, where $n=0,\pm1,\pm2,\ldots$. For any pair of scalar sources separated by a distance $l_1$ in the $x_1$ direction, the dimensional reaction rate integral [Eq. (11)] yields

$$\tilde{\Theta} = \frac{\sqrt{3}k}{8\pi\sigma Dt^2}\exp\left(-\frac{3l_1^2}{8\sigma^2 Dt^3}\right). \tag{18}$$

Summing over all periodic images yields an expression in terms of the Jacobi elliptic theta function, $\vartheta_2[0,q]$.[28] The resulting nondimensional reaction rate integral [Eq. (12)] becomes

$$\Theta(t) = \mathrm{Da}\frac{\sqrt{3}e}{\mathrm{Pe}}\frac{\vartheta_2[0,q]}{t^2}, \tag{19}$$

where $q=\exp(-3\pi^2\,\mathrm{Pe}^{-2}\,t^{-3})$. Defining self-similar variables

$$\Theta_s = \Theta\,\mathrm{Da}^{-1}\,\mathrm{Pe}^{-1/3} \quad \text{and} \quad t_s = t\,\mathrm{Pe}^{2/3} \tag{20}$$

permits Eq. (19) to be written as

$$\Theta_s(t_s) = \frac{\sqrt{3}e}{t_s^2}\vartheta_2[0,\exp(-3\pi^2 t_s^{-3})], \tag{21}$$

showing that for large Pe and small Da, the reaction rate collapses to a self-similar form. A plot of this solution for Pe$=10\,000$ is shown in Fig. 6(b).

## V. NUMERICAL SIMULATIONS

### A. Methodology

The reaction problem described in Secs. II and III, and solved analytically for special cases in Sec. IV, is now modeled numerically for general cases using a Lagrangian particle tracking method.[29] Each of the two scalars is represented by a collection of $N_p$ particles that advect passively with the local velocity and diffuse via a random walk. Particle positions $\mathbf{x}_i$ at time step $t_i$ are calculated as

$$\mathbf{x}_i = \mathbf{x}_{i-1} + \mathbf{u}(\mathbf{x}_{i-1})\Delta t + \mathbf{Z}\sqrt{2D\Delta t_i}, \tag{22}$$

where $\mathbf{x}_{i-1}$ and $\mathbf{u}_{i-1}$ are the particle positions and local velocities at the previous time step, $\Delta t_i = t_i - t_{i-1}$, and $\mathbf{Z}$ is a two-dimensional Gaussian process with zero mean and unity variance.

Particle locations are used to compute concentration fields for each scalar through spatial binning of particles at each time step. Individual particles are tagged with initial scalar mass $M/N_p$, and bin concentrations are calculated as total scalar mass in the bin divided by bin area. Although the particle domain is infinite, concentration binning is restricted to a finite region that is large enough such that it contains the vast majority of particles. Local reaction rates are then calculated using Eq. (4), and particle scalar masses in each bin are adjusted at each time step to reflect reactant loss.

Convergence of the $\Theta$ simulations is achieved based on suitable choice of $\Delta t_i$, $N_p$, and concentration bin size for a given Pe and Da. Time steps are chosen via a forward Euler approach such that the percent concentration change in any bin before the reaction step does not exceed a set threshold $\Delta C/C$. Typical parameters for a converged $\Theta$ solution are $N_p=10^5$, $\Delta C/C=0.05$, with $150\times150$ concentration bins spanning the central $2L\times2L$ region of the domain.

Snapshots of particle locations at five times within a representative simulation (Pe$=100$, Da$=1$, $E=0$, and $\phi=\pi$) are shown in the top row of Fig. 5. The resulting $\Theta$ versus $t$

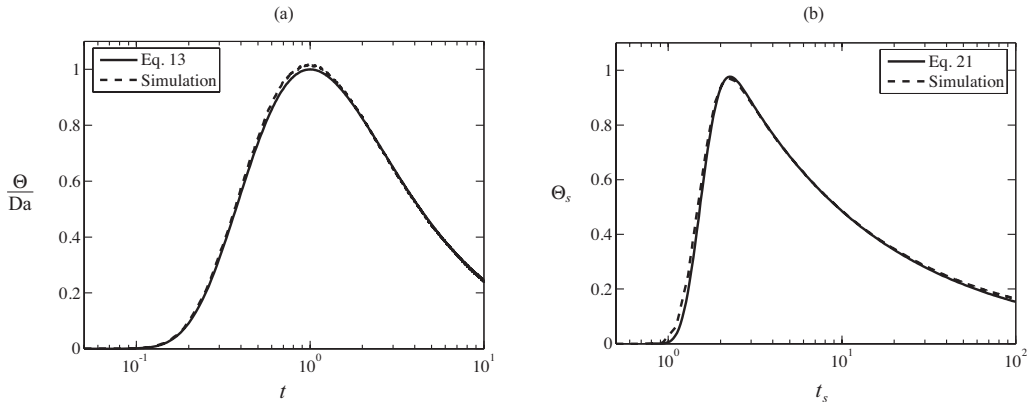


FIG. 6. Comparison of simulation results (dashed lines) with analytical solutions (solid lines). (a) Simulation at Pe=0, Da=0.01 compared to Eq. (13) and (b) simulation at Pe=10 000, Da=0.01 compared to Eq. (21).

curve for the same simulation is shown below the snapshots, and the time correspondence between the snapshots and the curve is indicated with dashed lines. At early times (the first two frames), the scalars are advected and strained into filaments by the vortex flow, but there are essentially no locations with co-occurring concentrations, and $\Theta$ remains negligibly small. At intermediate times (third and fourth frames), the vortex wraps the scalar filaments into increasingly close proximity such that diffusion can bridge the radial gap, and $\Theta$ rises and peaks. At long times (fifth frame), diffusion eradicates the scalar structure imposed by the vortex, and $\Theta$ asymptotes back to zero. This general behavior occurs for all values of Pe and Da.

Validation of the numerical model results at the low-Da limit is achieved by comparison with analytical solutions developed in Sec. IV. Excellent agreement is seen for Pe=0 [Eq. (13), Fig. 6(a)] and in the high-Pe limit [Eq. (21), Fig. 6(b)].

## B. Results

### 1. Effect of Pe

When Pe=0, the mixing process is purely diffusive, and the nondimensional reaction rates $\Theta$ are minimized. By the time diffusion alone bridges the distance $L$ between the two scalars, local concentrations and associated reaction rates are small throughout the domain. As Pe increases, the ratio of the diffusive to advective time scales increases, such that scalar filaments are more concentrated as vortex stirring more rapidly brings the two scalars into close proximity. Higher Pe numbers thus produce peak reaction rates $\Theta_{peak}$ that are larger, and that occur at smaller $t$ (Fig. 7).

In the slow reaction limit (Da$\ll$1), the purely diffusive case (Pe=0) has a peak reaction rate $\Theta_{peak}$=Da that occurs $t$=1. This serves as a baseline for the effect of vortex stirring on the reaction rates. It is thus convenient to normalize the nondimensional reaction rates by Da such that $\Theta_{peak}/\mathrm{Da}=1$ for Pe=0 and Da$\ll$1. This normalization is shown on the right-hand axis in Fig. 7 and is used extensively in the remainder of the paper. For a small, fixed Da, the value of $\Theta_{peak}/\mathrm{Da}$ indicates the factor by which vortex stirring increases nondimensional reaction rates relative to the pure diffusive case.

### 2. Effect of Da

The Damköhler number is a nondimensional form of the reaction rate constant $k$ [Eq. (4)]. Increases in Da therefore produce larger reaction rates $\Theta$ [Fig. 8(a)]. For Da$\ll$1, the increase in $\Theta_{peak}$ is linear with Da, but the increase is less than linear at higher Da due to the resulting reactant depletion. This effect is evident in Fig. 8(b), where $\Theta/\mathrm{Da}$ decreases with increasing Da. The $\Theta/\mathrm{Da}$ normalization removes the direct effect of $k$ in Eq. (4), revealing the secondary effect of reactant depletion. This same effect causes $t_{peak}$ to decrease with Da, but the effect is quite weak compared to that of Pe.

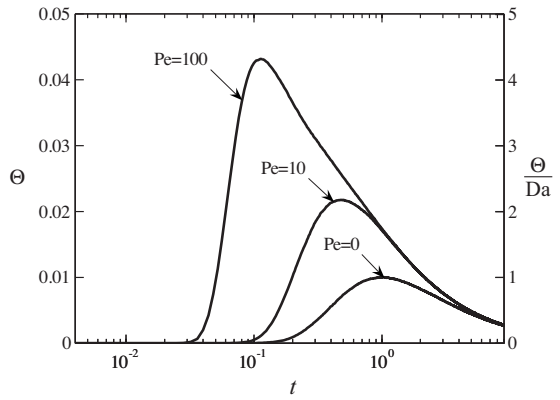


FIG. 7. Effect of Pe on the reaction rates for the symmetric initial condition ($E$=0, $\phi=\pi$). The simulations here are for Da=0.01, which is within the slow reaction regime. The left-hand axis shows nondimensional $\Theta$, and the right-hand axis shows the normalized value $\Theta/\mathrm{Da}$. When Pe=0 and Da$\ll$1, the normalized peak value is $\Theta_{peak}/\mathrm{Da}=1$, occurring at nondimensional time $t$=1.

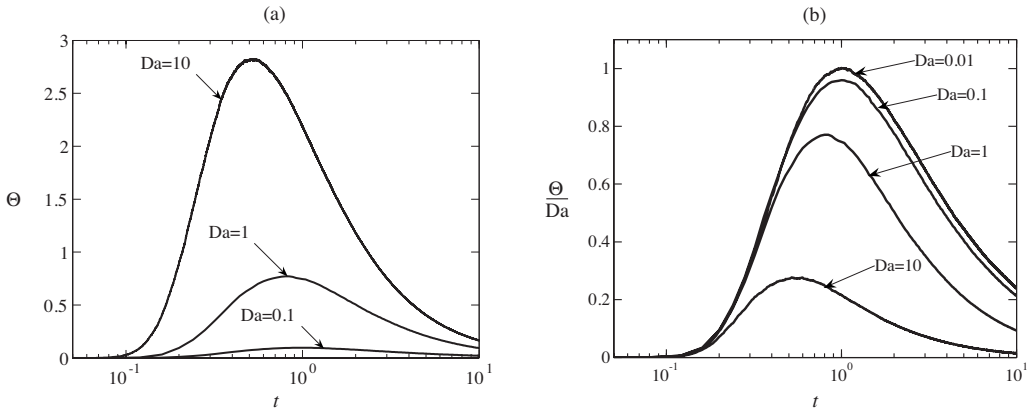


FIG. 8. Effect of Da on the reaction rates for the symmetric initial condition ($E=0$, $\phi=\pi$) in the case of pure diffusion (Pe=0). Simulation results are shown for (a) nondimensional reaction rate $\Theta$ and (b) normalized reaction rates $\Theta/\mathrm{Da}$. The latter result shows the effect of reactant depletion at higher Da.

### 3. Scaling relationships for $\Theta_{peak}$ and $t_{peak}$

Since the general behavior of $\Theta$ versus $t$ is similar for all values of Pe and Da, it is useful to focus our attention on the peak reaction values $\Theta_{peak}$ and $t_{peak}$. Motivated by the analytical results in Sec. IV, simulation results are used in this section to illustrate how these peak delimiters scale with Pe and Da in various regimes, again for the symmetric initial condition ($E=0$, $\phi=\pi$). In all cases, the nondimensional peak reaction rate is normalized as $\Theta_{peak}/\mathrm{Da}$. As discussed above, this removes the direct multiplicative effect of $k$ in Eq. (4), and also establishes $\Theta_{peak}/\mathrm{Da}=1$ as the baseline peak reaction rate for Pe=0 and $\mathrm{Da}\ll 1$.

In Sec. IV, analytical results indicate that $\Theta_{peak}/\mathrm{Da}\sim \mathrm{Pe}^{1/3}$ and $t_{peak}\sim \mathrm{Pe}^{-2/3}$ in the limit $\mathrm{Pe}\gg 1$ and $\mathrm{Da}\ll 1$. Simulation results are consistent with this scaling, as shown in Fig. 9. At high Pe, $\Theta_{peak}/\mathrm{Da}$ simulations scale as $\mathrm{Pe}^{1/3}$ and are insensitive to Da [Fig. 9(a)], and $t_{peak}$ simulations scale as $\mathrm{Pe}^{-2/3}$ and are likewise insensitive to Da [Fig. 9(b)]. As $\mathrm{Pe}\to 0$, the simulations deviate from this scaling as $\Theta_{peak}/\mathrm{Da}$ and $t_{peak}$ asymptote to their purely diffusive limits. For low Da, this corresponds to $\Theta_{peak}/\mathrm{Da}=1$ and $t_{peak}=1$, but both values are reduced at higher Da due to early reactant depletion. The simulations indicate that the high-Pe scaling relationships are not limited to low Da as long as Pe is sufficiently high.

The $\Theta_{peak}\sim \mathrm{Da}$ scaling predicted at low Da can be seen explicitly by examining the simulation results of $\Theta_{peak}/\mathrm{Da}$ versus Da [Fig. 10(a)]. As $\mathrm{Da}\to 0$, $\Theta_{peak}/\mathrm{Da}$ asymptotes to a constant that depends on Pe. At higher Da, the $\Theta_{peak}\sim \mathrm{Da}$ scaling breaks down due to reactant depletion. The Pe dependence can be removed for high Pe by using a scaling of $\Theta_{peak}/(\mathrm{Da}\,\mathrm{Pe}^{1/3})$ [suggested by $\Theta_s$ in Eq. (21)], as shown in Fig. 10(b). Once again, it is seen that the smallness of Da required for the asymptotic low-Da behavior is less stringent at high Pe.

Simulation results for $t_{peak}$, analogous to those shown in the previous figure for $\Theta_{peak}$, are shown in Fig. 11. As $\mathrm{Da}\to 0$, $t_{peak}$ asymptotes to a constant that depends on Pe [Fig. 11(a)]. The range over which this asymptote remains constant increases with Pe, such that $t_{peak}$ is relatively insensitive to Da at low Da or at high Pe. The Pe dependence of the asymptotic value of $t_{peak}$ can be removed for high Pe by using a scaling of $t_{peak}\,\mathrm{Pe}^{2/3}$ [suggested by $t_s$ in Eq. (21)], as shown in Fig. 11(b).

### 4. Effect of initial conditions

Numerical simulations on the effect of radial eccentricity on reaction rates $\Theta/\mathrm{Da}$ are shown in Fig. 12 for the angularly symmetric case $\phi=\pi$ at Pe=100. For small radial eccentricities (approximately $E\leq 0.2$), the peak reaction rates

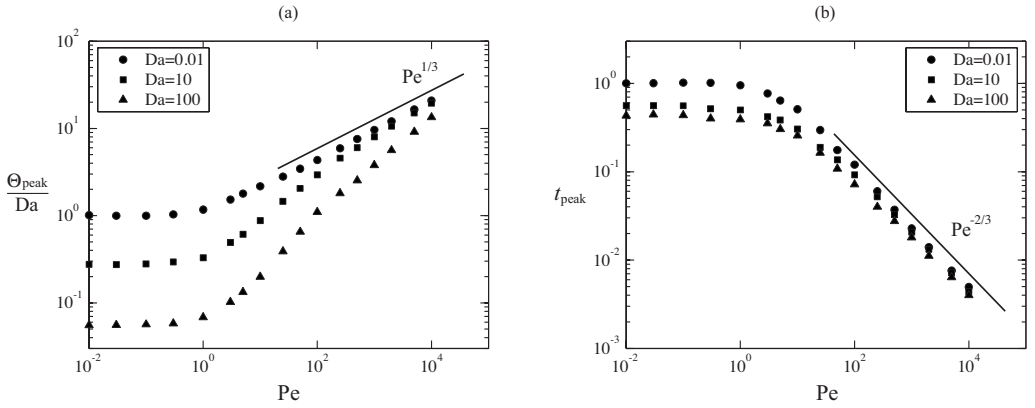


FIG. 9. Péclet scaling for (a) normalized peak reaction rates $\Theta_{peak}/\mathrm{Da}$ and (b) peak reaction times $t_{peak}$. Simulations results are shown as symbols, and reference scaling slopes $\mathrm{Pe}^{1/3}$ and $\mathrm{Pe}^{-2/3}$ are shown as lines.

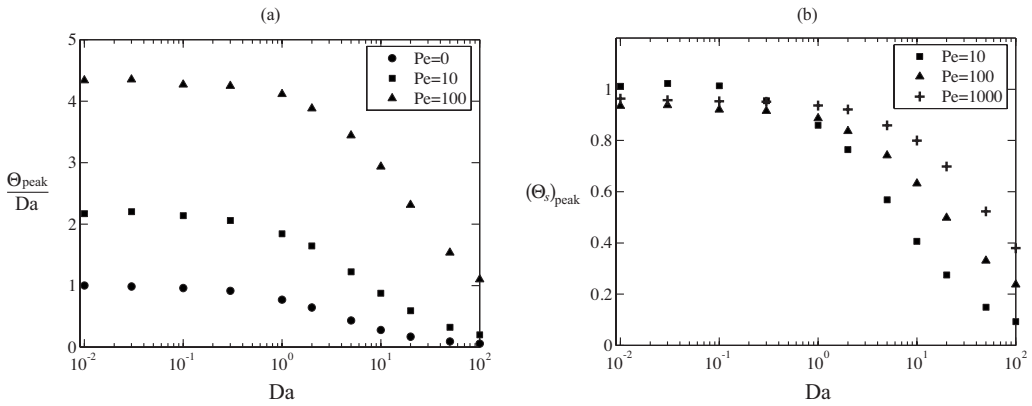


FIG. 10. Damköhler scaling for peak reaction rates. Simulation results are plotted as (a) normalized reaction rate $\Theta_{peak}/Da$ and (b) self-similar reaction rates $\Theta_s$ [see Eq. (21)].

are enhanced beyond the symmetric case $E=0$, and the peak occurs at smaller nondimensional times. At larger radial eccentricities, $\Theta_{peak}$ is reduced. In the limit as $E \to 1$, the reaction rates for any Pe regress back to the purely diffusive solution [compare the $E=1$ results in Figs. 12(a) and 12(b) with those shown in Fig. 8(b)]. Moderate values of radial asymmetry alter the evolution of $\Theta$ such that there are two local reaction rate maxima. Larger values of Da [Fig. 12(b)] favor the first peak over the second due to reactant limitations at larger times (compare the two $E=0.3$ curves).

The mechanisms responsible for producing dual maxima at moderate $E$ values are shown in Fig. 13 for $E=0.15$, Pe $=1000$, Da$=0.05$, and $\phi=\pi$. The first maximum is driven by asymmetric stirring and corresponds to the leading edge of the outer filament catching the trailing edge of the inner filament. The second maximum is driven by radial diffusion after the outer scalar has been well distributed in the circumferential direction.

The effect of angular eccentricity $\phi$ on peak nondimensional reaction rates is relatively small, as shown in Fig. 14. All simulations of $\Theta_{peak}/Da$ exhibit a local minimum at $\phi = \pi/2$, with the effect of $\phi$ becoming larger as Pe increases.

### 5. Effect of vortex type

The acceleration and enhancement of reaction rates due to vortex stirring seen in this study are linked to circumferential strain associated with the radial distribution of the velocity field. The effect of strain can be emphasized by replacing the point vortex flowfield [Eq. (2)] with a Lamb–Oseen vortex of the form

$$u_\phi(r) = \frac{\Gamma}{2\pi r}\left\{1 - \exp\left[-\left(\frac{r}{R_c}\right)^2\right]\right\}, \tag{23}$$

where $R_c$ is the radius of the rotational vortex core. For $r \ll R_c$, the vortex exhibits a solid-body rotation with no strain, and for $r \gg R_c$, the vortex behaves as a point vortex. The effect of the vortex on reaction rate enhancement thus depends on the radial placement of the scalars relative to the vortex core. Simulation results for $\Theta_{peak}/Da$ as a function of the initial scalar location $L/2R_c$ are shown in Fig. 15 for Pe$=1000$ for the symmetric case $E=0$ and $\phi=\pi$. When $L/2R_c \ll 1$, the initial scalar placement is within the rotational vortex core. Since there is no strain, the reaction rates (symbols) asymptote to those found previously for pure dif-

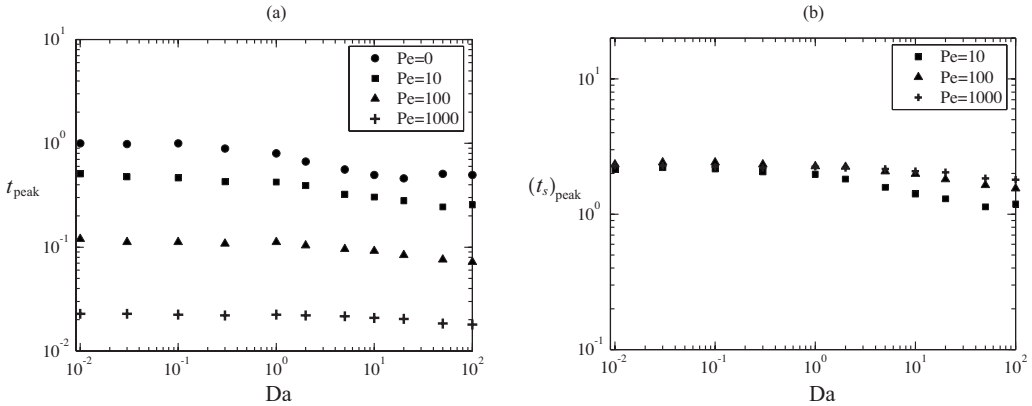


FIG. 11. Damköhler scaling for peak reaction times. Simulation results are plotted as (a) nondimensional peak reaction time $t_{peak}$ and (b) self-similar reaction time $t_s$ [see Eq. (21)].

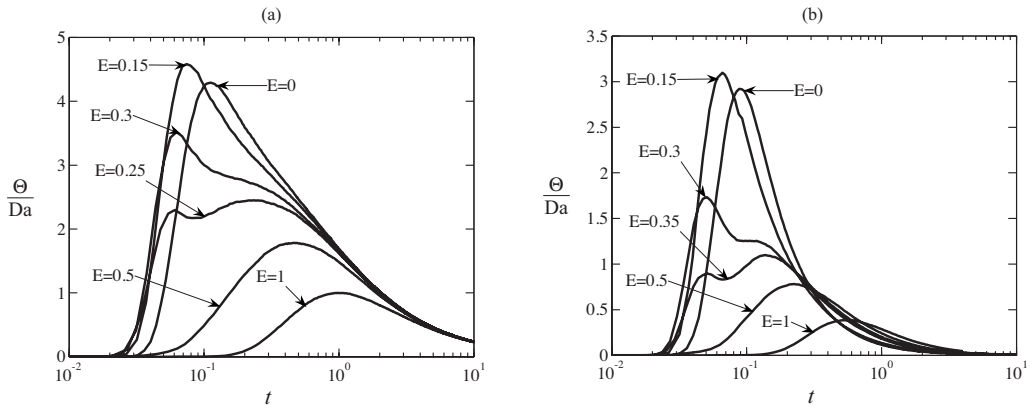


FIG. 12. Effect of radial eccentricity on the evolution of Θ in the case of (a) the low-Da limit with Da=0.05 and (b) for a faster reaction scenario where Da=10. In both cases, Pe=100, and the initial scalar condition is angularly symmetric ($\phi=\pi$).

fusion (shown with dashed lines). When $L/2R_c \gg 1$, the initial scalar placement is in the straining tail of the vortex, and the reaction rates equal those found for a point vortex.

## VI. SUMMARY AND DISCUSSION

The analytical and numerical results presented herein demonstrate the effect of stirring by a single vortex on reaction rates between two isolated scalar sources. The scalar configuration differs from previous studies in that the reactants are initially separated by ambient fluid that acts as a third nonreactive scalar. When molecular diffusion alone disperses the reactants (Pe=0), the nondimensional reaction rate Θ is minimized, and the nondimensional time to the peak reaction rate $t_{peak}$ is maximized. The presence of vortex stirring (Pe>0) always acts to increase Θ and decrease $t_{peak}$. These findings are true regardless of the value of Da and of the initial scalar geometry ($E$ and $\phi$).

Several general scaling relationships are shown to hold. For high Péclet numbers, the peak reaction rate $\Theta_{peak}$ scales as $Pe^{1/3}$, and the peak time $t_{peak}$ scales as $Pe^{-2/3}$. These scaling relationships were found analytically for the slow reaction limit ($Da \ll 1$). However, for the regime $Pe \gg Da$, one can argue that the scaling regime applies even if Da is not small. The calculation presented above describes the motion of fluid parcels regardless of their chemical reactions. If $Pe \gg Da$, then the reactions are slow compared to advection, reactant depletion can be ignored over advective time scales, and peak reaction rates and peak reaction times should scale as in the $Da \ll 1$ case. The numerical simulations suggest agreement with an extension of the scaling result to $Pe \gg Da \gtrsim 1$, but we have not reached a sufficient separation of Pe and Da to conclusively show this. The peak reaction rate was also shown to scale linearly with Da in the slow reaction limit. Reaction rates fall short of this scaling at higher Da due to reactant depletion.

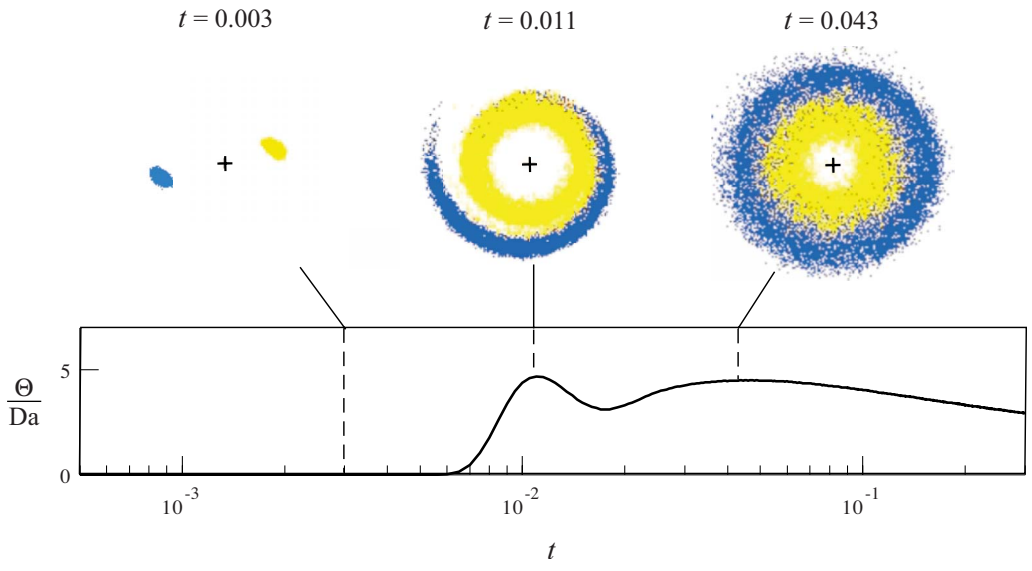


FIG. 13. (Color online) Mechanisms for dual reaction rate maxima in the case radial eccentricity $E=0.15$. Particle locations at three simulation times for scalars $A$ [light gray (yellow online)] and $B$ [dark gray (blue online)] for the case Pe=1000, Da=0.05, and $\phi=\pi$. Also shown is the associated Θ vs $t$ simulation result for a continuous range of times with the corresponding snapshot times indicated as dashed lines. The two final times ($t=0.011$ and $t=0.043$) correspond to the local maxima. For clarity, these results are shown at a higher Pe than those shown in Fig. 12.

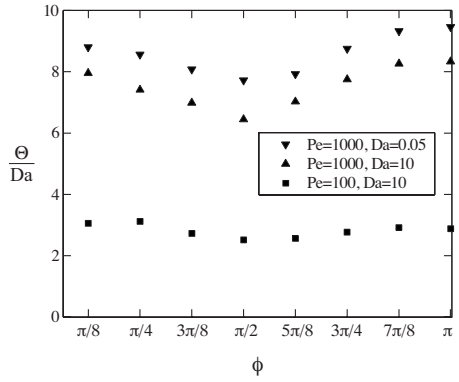


FIG. 14. Effect of angular asymmetry on peak reaction rates $\Theta_{peak}/Da$. The initial scalar condition is radially symmetric ($E=0$) in all cases.

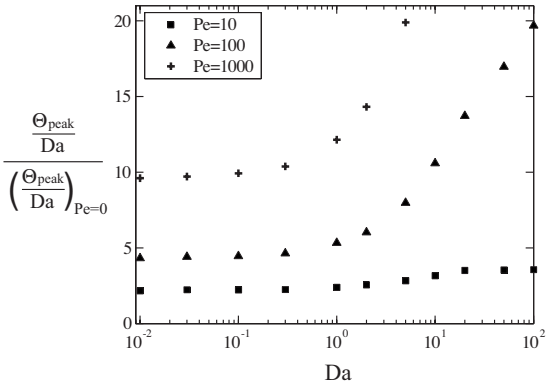


FIG. 16. Effect of Da on the ratio of stirred to unstirred values of $\Theta_{peak}/Da$. The stirred and unstirred results are shown separately in Fig. 10.

It is important to note that an increase in $\Theta$ does not automatically correspond to an increase in the dimensional reaction rate $\tilde{\Theta}$. For example, a decrease in scalar diffusivity $D$ reduces the dimensional reaction rate $\tilde{\Theta}$ for both stirred and unstirred cases due to reduced reactant mixing. However, this diffusivity decrease increases Pe and therefore $\Theta$. The increase in $\Theta$ indicates that the ratio of dimensional stirred reaction rates to dimensional unstirred rates is larger at the lower diffusivity, even though both dimensional rates are lower. On the other hand, an increase in Pe due to increased vortex strength $\Gamma$ results in increases in both $\tilde{\Theta}$ and $\Theta$.

Reaction rates were nondimensionalized in a way that references them to the unstirred case in the slow reaction limit. Thus, for $Da \ll 1$, $\Theta/Da$ is the factor by which dimensional reaction rates are enhanced by vortex stirring. It turns out that, at higher Da, the factor by which stirring enhances reaction rates is even larger than $\Theta/Da$. To see this, consider the reaction rate curves in Fig. 10(a). At low Da, the $\Theta/Da$ value for a given Pe is simply the reaction enhancement factor since $\Theta/Da$ for the unstirred case at low Da is unity. As Da increases, the stirred $\Theta/Da$ values decrease, but the unstirred $\Theta/Da$ values decrease at an even faster rate. Thus, the ratio of stirred to unstirred reaction rates increases as Da increases. This effect is shown in Fig. 16, which is the same as Fig. 10(a) except that each curve is normalized by the Pe=0 curve. As Pe and Da increase, the relative reaction enhancement increases dramatically.

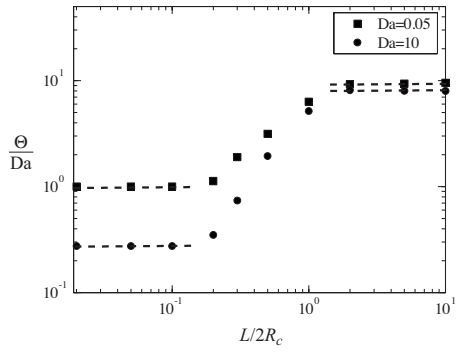


FIG. 15. Peak reaction rates within a Lamb–Oseen vortex [Eq. (23)] at Pe =1000 for a symmetric condition $E=0$ and $\phi=\pi$. The ratio $L/2R_c$ describes the initial separation of the scalars relative to the radius of the rotational vortex core $R_c$. The dashed lines on the left and right sides indicate the reaction rate limits for pure diffusion and for a point vortex, respectively.

The results have important implications for modeling of systems with initially distinct scalars. Since $\Theta/Da$ is a measure of the reaction rate enhancement produced by stirring relative to a purely diffusive process, $\Theta_{peak}/Da$ is always at the minimum possible value of unity for any purely diffusive process, even if the diffusivity $D$ is replaced by a much larger effective turbulent diffusivity. The implication is that reactions between initially isolated scalars will be underpredicted by any scheme using an effective diffusivity since the scalar correlations imposed by coherent vortex structures are not captured.[25] This shortcoming is well understood for problems of the first topological class, but the present study extends the concept to a specific problem in the second topological class. Nonetheless, it is easy to imagine configurations within the second class of problems where vortex stirring will not enhance reactions, and generalizations about the effect of stirring on problems within the second class are not yet possible.

## ACKNOWLEDGMENTS

This work was supported by the National Science Foundation under CAREER Grant No. 0348855.

[1] B. M. Cetegen and W. A. Sirignano, "Study of mixing and reaction in the field of a vortex," Combust. Sci. Technol. **72**, 157 (1990).
[2] B. M. Cetegen and N. Mohamad, "Experiments on liquid-mixing and reaction in a vortex," J. Fluid Mech. **249**, 391 (1993).
[3] R. G. Rehm, H. R. Baum, H. C. Tang, and D. C. Lozier, "Finite-rate diffusion-controlled reaction in a vortex," Combust. Sci. Technol. **91**, 143 (1993).
[4] P. Flohr and J. C. Vassilicos, "Accelerated scalar dissipation in a vortex," J. Fluid Mech. **348**, 295 (1997).
[5] K. Bajer, A. P. Bassom, and A. D. Gilbert, "Accelerated diffusion in the centre of a vortex," J. Fluid Mech. **437**, 395 (2001).
[6] J. C. Vassilicos, "Mixing in vortical, chaotic and turbulent flows," Philos. Trans. R. Soc. London, Ser. A **360**, 2819 (2002).
[7] P. Meunier and E. Villermaux, "How vortices mix," J. Fluid Mech. **476**, 213 (2003).
[8] S. Basu, T. J. Barber, and B. M. Cetegen, "Computational study of scalar mixing in the field of a gaseous laminar line vortex," Phys. Fluids **19**, 053601 (2007).

[9]D. Martinand and J. C. Vassilicos, "Fast chemical reaction and multiple-scale concentration fields in singular vortices," Phys. Rev. E **75**, 036315 (2007).
[10]J. M. Ottino, "Mixing and chemical reactions: A tutorial," Chem. Eng. Sci. **49**, 4005 (1994).
[11]S. Edouard, B. Legras, and V. Zeitlin, "The effect of dynamical mixing in a simple model of the ozone hole," J. Geophys. Res., [Atmos.] **101**, 16771, DOI: 10.1029/96JD00856 (1996).
[12]F. J. Muzzio and M. Liu, "Chemical reactions in chaotic flows," Chem. Eng. J. **64**, 117 (1996).
[13]M. J. Clifford, S. M. Cox, and E. P. L. Roberts, "Lamellar modelling of reaction, diffusion and mixing in a two-dimensional flow," Chem. Eng. J. **71**, 49 (1998).
[14]D. G. H. Tan, P. H. Haynes, A. R. MacKenzie, and J. A. Pyle, "Effects of fluid-dynamical stirring and mixing on the deactivation of stratospheric chlorine," J. Geophys. Res., [Atmos.] **103**, 1585, DOI: 10.1029/97JD02495 (1998).
[15]J. M. Zalc and F. J. Muzzio, "Parallel-competitive reactions in a two-dimensional chaotic flow," Chem. Eng. Sci. **54**, 1053 (1999).
[16]W. Gerlinger, K. Schneider, L. Falk, and H. Bockhorn, "Numerical simulation of the mixing of passive and reactive scalars in two-dimensional flows dominated by coherent vortices," Chem. Eng. Sci. **55**, 4255 (2000).
[17]M. Chertkov and V. Lebedev, "Boundary effects on chaotic advection-diffusion chemical reactions," Phys. Rev. Lett. **90**, 134501 (2003).
[18]S. M. Cox, "Chaotic mixing of a competitive-consecutive reaction," Physica D **199**, 369 (2004).
[19]T. Tél, A. de Moura, C. Grebogi, and G. Karolyi, "Chemical and biological activity in open flows: A dynamical system approach," Phys. Rep. **413**, 91 (2005).
[20]C. Day, "Experiment tracks and progress of a chaotically mixed chemical reaction," Phys. Today **59**(2), 15 (2006).
[21]G. Károlyi and T. Tél, "Effective dimensions and chemical reactions in fluid flows," Phys. Rev. E **76**, 046315 (2007).
[22]P. B. Rhines and W. R. Young, "How rapidly is a passive scalar mixed within closed streamlines," J. Fluid Mech. **133**, 133 (1983).
[23]D. R. Levitan, "The ecology of fertilization in free-spawning invertebrates," in *Ecology of Marine Invertebrate Larvae*, edited by L. R. McEdward (CRC, Boca Raton, 1995), pp. 123–156.
[24]M. W. Denny, *Biology and the Mechanics of the Wave-Swept Environment* (Princeton University Press, Princeton, NJ, 1988).
[25]J. P. Crimaldi and H. S. Browning, "A proposed mechanism for turbulent enhancement of broadcast spawning efficiency," J. Mar. Syst. **49**, 3 (2004).
[26]J. P. Crimaldi, J. R. Hartford, and J. B. Weiss, "Reaction enhancement of point sources due to vortex stirring," Phys. Rev. E **74**, 016307 (2006).
[27]N. G. V. Kampen, *Stochastic Processes in Physics and Chemistry* (Elsevier, Amsterdam, 2007).
[28]M. Abramowitz and I. A. Stegun, *Handbook of Mathematical Functions* (Dover, New York, 1974).
[29]W. Kinzelbach, "The random walk method in pollutant transport simulation," in *Groundwater Flow and Quality Modeling*, edited by E. Custodio (Reidel, Rotterdam, 1988), pp. 227–245.